Biomedical Optics EXPRESS

A new broadband near-infrared spectroscopy system for in-vivo measurements of cerebral cytochrome-c-oxidase changes in neonatal brain injury

Gemma Bale,[1*] Subhabrata Mitra,[2] Judith Meek,[2] Nicola Robertson,[2] and Ilias Tachtsidis[1]

[1]*Department of Medical Physics and Bioengineering, Malet Place Engineering Building, University College London, UK*

[2]*Institute for Women's Health, University College London and Neonatal Unit, University College London Hospitals Trust, London, UK*

[*]*gemma.bale.11@ucl.ac.uk*

Abstract: We present a novel lens-based broadband near-infrared spectroscopy system to simultaneously measure cerebral changes in tissue oxygenation and haemodynamics via estimation of the changes in haemoglobin concentration; in addition to oxygen utilization via the measurement of the oxidation state of cytochrome-c-oxidase (CCO). We demonstrate the use of the system in a cohort of 6 newborn infants with neonatal encephalopathy in the Neonatal Intensive Care Unit for continuous measurement periods of up to 5 days. NIRS data was collected from above the frontal lobe on the left and right hemispheres simultaneously with systemic data to allow multimodal data analysis. This allowed us to study the NIRS variables in response to global pathophysiological events and we focused our analysis to spontaneous oxygen desaturations. We identified changes from the NIRS variables during 236 oxygen desaturations from over 212 hours of data with a change from the baseline to nadir of −12 ± 3%. There was a consistent negative change in the Δ[HbD] (= oxygenated – deoxygenated haemoglobin) and Δ[oxCCO] measurements, mean decreases were 3.0 ± 1.7μM and 0.22 ± 0.11μM, and a positive change in the Δ[HbT] (= oxygenated + deoxygenated haemoglobin) measurements across all subjects, mean increase was 0.85 ± 0.58μM. We have shown with a feasibility study that the relationship between haemoglobin oxygenation changes and CCO oxidation changes during these desaturation events was significantly associated with a magnetic resonance spectroscopy (MRS)-measured biomarker of injury severity ($r = 0.91$, $p<0.01$).

OCIS codes: (170.6510) Spectroscopy, tissue diagnostics; (170.3890) Medical optics instrumentation.

References and Links

1. F. Scholkmann, S. Kleiser, A. J. Metz, R. Zimmermann, J. Mata Pavia, U. Wolf, and M. Wolf, "A review on continuous wave functional near-infrared spectroscopy and imaging instrumentation and methodology," Neuroimage **85**(Pt 1), 6–27 (2014).
2. M. Wolf and G. Greisen, "Advances in near-infrared spectroscopy to study the brain of the preterm and term neonate," Clin. Perinatol. **36**(4), 807–834 (2009).
3. D. A. Boas and M. A. Franceschini, "Haemoglobin oxygen saturation as a biomarker: the problem and a solution," Philos. Trans. A Math Phys. Eng. Sci. **369**(1955), 4407–4424 (2011).
4. F. Zheng, R. Sheinberg, M.-S. Yee, M. Ono, Y. Zheng, and C. W. Hogue, "Cerebral near-infrared spectroscopy monitoring and neurologic outcomes in adult cardiac surgery patients: a systematic review," Anesth. Analg. **116**(3), 663–676 (2013).

#214019 - $15.00 USD Received 12 Jun 2014; revised 15 Aug 2014; accepted 22 Aug 2014; published 5 Sep 2014

5. G. Naulaers, B. Meyns, M. Miserez, V. Leunens, S. Van Huffel, P. Casaer, M. Weindling, and H. Devlieger, "Use of tissue oxygenation index and fractional tissue oxygen extraction as non-invasive parameters for cerebral oxygenation. A validation study in piglets," Neonatology **92**(2), 120–126 (2007).
6. F. van Bel, P. Lemmers, and G. Naulaers, "Monitoring neonatal regional cerebral oxygen saturation in clinical practice: value and pitfalls," Neonatology **94**(4), 237–244 (2008).
7. N. Roche-Labarbe, S. A. Carp, A. Surova, M. Patel, D. A. Boas, P. E. Grant, and M. A. Franceschini, "Noninvasive optical measures of CBV, StO2, CBF index, and rCMRO2 in human premature neonates' brains in the first six weeks of life," Hum. Brain Mapp. **31**(3), 341–352 (2010).
8. M. Dehaes, A. Aggarwal, P.-Y. Lin, C. Rosa Fortuno, A. Fenoglio, N. Roche-Labarbe, J. S. Soul, M. A. Franceschini, and P. E. Grant, "Cerebral oxygen metabolism in neonatal hypoxic ischemic encephalopathy during and after therapeutic hypothermia," J. Cereb. Blood Flow Metab. **34**(1), 87–94 (2014).
9. H. Z. Yeganeh, V. Toronov, J. T. Elliott, M. Diop, T.-Y. Lee, and K. St. Lawrence, "Broadband continuous-wave technique to measure baseline values and changes in the tissue chromophore concentrations," Biomed. Opt. Express **3**(11), 2761–2770 (2012).
10. A. D. Edwards, P. Brocklehurst, A. J. Gunn, H. Halliday, E. Juszczak, M. Levene, B. Strohm, M. Thoresen, A. Whitelaw, and D. Azzopardi, "Neurological outcomes at 18 months of age after moderate hypothermia for perinatal hypoxic ischaemic encephalopathy: synthesis and meta-analysis of trial data," Brit. Med. J **340**, c363 (2010).
11. S. J. Matcher, C. E. Elwell, C. E. Cooper, M. Cope, and D. T. Delpy, "Performance comparison of several published tissue near-infrared spectroscopy algorithms," Anal. Biochem. **227**(1), 54–68 (1995).
12. I. Tachtsidis, M. Tisdall, T. S. Leung, C. E. Cooper, D. T. Delpy, M. Smith, and C. E. Elwell, "Investigation of in vivo measurement of cerebral cytochrome-c-oxidase redox changes using near-infrared spectroscopy in patients with orthostatic hypotension," Physiol. Meas. **28**(2), 199–211 (2007).
13. P. P. Drury, L. Bennet, L. C. Booth, J. O. Davidson, G. Wassink, and A. J. Gunn, "Maturation of the mitochondrial redox response to profound asphyxia in fetal sheep," PLoS ONE **7**(6), e39273 (2012).
14. M. M. Tisdall, I. Tachtsidis, T. S. Leung, C. E. Elwell, and M. Smith, "Near-infrared spectroscopic quantification of changes in the concentration of oxidized cytochrome c oxidase in the healthy human brain during hypoxemia," J. Biomed. Opt. **12**(2), 024002 (2007).
15. I. Tachtsidis, M. M. Tisdall, C. Pritchard, T. S. Leung, A. Ghosh, C. E. Elwell, and M. Smith, "Analysis of the Changes in the Oxidation of Brain Tissue Cytochrome-c-Oxidase in Traumatic Brain Injury Patients During Hypercapnoea: A Broadband NIRS Study," Adv. Exp. Med. Biol. **701**, 9–14 (2011).
16. A. Ghosh, I. Tachtsidis, C. Kolyva, C. E. Cooper, M. Smith, and C. E. Elwell, "Use of a hybrid optical spectrometer for the measurement of changes in oxidized cytochrome c oxidase concentration and tissue scattering during functional activation," Adv. Exp. Med. Biol. **737**, 119–124 (2012).
17. A. Ghosh, I. Tachtsidis, C. Kolyva, D. Highton, C. Elwell, and M. Smith, "Normobaric hyperoxia does not change optical scattering or pathlength but does increase oxidised cytochrome C oxidase concentration in patients with brain injury," Adv. Exp. Med. Biol. **765**, 67–72 (2013).
18. J. Lee, J. Armstrong, K. Kreuter, B. J. Tromberg, and M. Brenner, "Non-invasive in vivo diffuse optical spectroscopy monitoring of cyanide poisoning in a rabbit model," Physiol. Meas. **28**(9), 1057–1066 (2007).
19. A. Bainbridge, I. Tachtsidis, S. D. Faulkner, D. Price, T. Zhu, E. Baer, K. D. Broad, D. L. Thomas, E. B. Cady, N. J. Robertson, and X. Golay, "Brain mitochondrial oxidative metabolism during and after cerebral hypoxia-ischemia studied by simultaneous phosphorus magnetic-resonance and broadband near-infrared spectroscopy," Neuroimage, doi:10.1016/j.neuroimage.2013.08.016 (2013).
20. C. E. Elwell and C. E. Cooper, "Making light work: illuminating the future of biomedical optics," Philos. Trans. A Math Phys. Eng. Sci. **369**(1955), 4358–4379 (2011).
21. N. N. Finer, C. M. Robertson, R. T. Richards, L. E. Pinnell, and K. L. Peters, "Hypoxic-ischemic encephalopathy in term neonates: perinatal factors and outcome," J. Pediatr. **98**(1), 112–117 (1981).
22. A. Lorek, Y. Takei, E. B. Cady, J. S. Wyatt, J. Penrice, A. D. Edwards, D. Peebles, M. Wylezinska, H. Owen-Reece, V. Kirkbride, C. E. Cooper, R. F. Aldridge, S. C. Roth, G. Brown, D. T. Delpy, and E. O. R. Reynolds, "Delayed ("secondary") cerebral energy failure after acute hypoxia-ischemia in the newborn piglet: continuous 48-hour studies by phosphorus magnetic resonance spectroscopy," Pediatr. Res. **36**(6), 699–706 (1994).
23. R. M. Pressler, G. B. Boylan, M. Morton, C. D. Binnie, and J. M. Rennie, "Early serial EEG in hypoxic ischaemic encephalopathy," Clin. Neurophysiol. **112**(1), 31–37 (2001).
24. P. E. Grant, N. Roche-Labarbe, A. Surova, G. Themelis, J. Selb, E. K. Warren, K. S. Krishnamoorthy, D. A. Boas, and M. A. Franceschini, "Increased cerebral blood volume and oxygen consumption in neonatal brain injury," J. Cereb. Blood Flow Metab. **29**(10), 1704–1713 (2009).
25. M. M. Tisdall, I. Tachtsidis, T. S. Leung, C. E. Elwell, and M. Smith, "Changes in the attenuation of near infrared spectra by the healthy adult brain during hypoxaemia cannot be accounted for solely by changes in the concentrations of oxy- and deoxy-haemoglobin," Adv. Exp. Med. Biol. **614**, 217–225 (2008).
26. C. Kolyva, I. Tachtsidis, A. Ghosh, T. Moroz, C. E. Cooper, M. Smith, and C. E. Elwell, "Systematic investigation of changes in oxidized cerebral cytochrome c oxidase concentration during frontal lobe activation in healthy adults," Biomed. Opt. Express **3**(10), 2550–2566 (2012).
27. A. Duncan, J. H. Meek, M. Clemence, C. E. Elwell, L. Tyszczuk, M. Cope, and D. T. Delpy, "Optical pathlength measurements on adult head, calf and forearm and the head of the newborn infant using phase resolved optical spectroscopy," Phys. Med. Biol. **40**(2), 295–304 (1995).
28. F. Scholkmann, S. Spichtig, T. Muehlemann, and M. Wolf, "How to detect and reduce movement artifacts in near-infrared imaging using moving standard deviation and spline interpolation," Physiol. Meas. **31**(5), 649–662 (2010).

#214019 - $15.00 USD Received 12 Jun 2014; revised 15 Aug 2014; accepted 22 Aug 2014; published 5 Sep 2014

29. K. Uludag, M. Kohl, J. Steinbrink, H. Obrig, and A. Villringer, "Cross talk in the Lambert-Beer calculation for near-infrared wavelengths estimated by Monte Carlo simulations," J. Biomed. Opt. **7**(1), 51–59 (2002).
30. K. Uludağ, J. Steinbrink, M. Kohl-Bareis, R. Wenzel, A. Villringer, and H. Obrig, "Cytochrome-c-oxidase redox changes during visual stimulation measured by near-infrared spectroscopy cannot be explained by a mere cross talk artefact," Neuroimage **22**(1), 109–119 (2004).
31. C. Kolyva, I. Tachtsidis, A. Ghosh, T. Moroz, C. E. Cooper, M. Smith, and C. E. Elwell, "Systematic investigation of changes in oxidized cerebral cytochrome c oxidase concentration during frontal lobe activation in healthy adults," Biomed. Opt. Express **3**(10), 2550–2566 (2012).
32. H. R. Heekeren, M. Kohl, H. Obrig, R. Wenzel, W. von Pannwitz, S. J. Matcher, U. Dirnagl, C. E. Cooper, and A. Villringer, "Noninvasive assessment of changes in cytochrome-c oxidase oxidation in human subjects during visual stimulation," J. Cereb. Blood Flow Metab. **19**(6), 592–603 (1999).
33. M. Diop, E. Wright, V. Toronov, T. Y. Lee, and K. St Lawrence, "Improved light collection and wavelet de-noising enable quantification of cerebral blood flow and oxygen metabolism by a low-cost, off-the-shelf spectrometer," J. Biomed. Opt. **19**(5), 057007 (2014).
34. O. Pucci, V. Toronov, and K. St Lawrence, "Measurement of the optical properties of a two-layer model of the human head using broadband near-infrared spectroscopy," Appl. Opt. **49**(32), 6324–6332 (2010).
35. Y. Sakata, M. Abajian, M. O. Ripple, and R. Springett, "Measurement of the oxidation state of mitochondrial cytochrome c from the neocortex of the mammalian brain," Biomed. Opt. Express **3**(8), 1933–1946 (2012).
36. M. Banaji, A. Mallet, C. E. Elwell, P. Nicholls, and C. E. Cooper, "A model of brain circulation and metabolism: NIRS signal changes during physiological challenges," PLOS Comput. Biol. **4**(11), e1000212 (2008).
37. A. D. Edwards, G. C. Brown, M. Cope, J. S. Wyatt, D. C. McCormick, S. C. Roth, D. T. Delpy, and E. O. Reynolds, "Quantification of concentration changes in neonatal human cerebral oxidized cytochrome oxidase," J. Appl. Physiol. **71**(5), 1907–1913 (1991).
38. P. Wintermark, A. Hansen, S. K. Warfield, D. Dukhovny, and J. S. Soul, "Near-infrared spectroscopy versus magnetic resonance imaging to study brain perfusion in newborns with hypoxic-ischemic encephalopathy treated with hypothermia," Neuroimage **85**(1), 287–293 (2014).
39. A. Caicedo, M. D. Papademetriou, C. E. Elwell, A. Hoskote, M. J. Elliott, S. Van Huffel, and I. Tachtsidis, "Canonical Correlation Analysis in the Study of Cerebral and Peripheral Haemodynamics Interrelations with Systemic Variables in Neonates Supported on ECMO," Adv. Exp. Med. Biol. **765**, 23–29 (2013).
40. S. Suzuki, S. Takasaki, T. Ozaki, and Y. Kobayashi, "A Tissue Oxygenation Monitor using NIR Spatially Resolved Spectroscopy," Proc. SPIE **3597**, 582–592 (1999).
41. A. Li, R. Kwong, A. Cerussi, S. Merritt, C. Hayakawa, and B. Tromberg, "Method for recovering quantitative broadband diffuse optical spectra from layered media," Appl. Opt. **46**(21), 4828–4833 (2007).

1. Introduction

Near-infrared spectroscopy (NIRS) is a non-invasive, non-ionizing technique that allows bedside in-vivo monitoring of changes of tissue chromophore concentrations and has been widely used in the study of both adult and neonatal brains [1]. NIRS systems are used to measure changes in the concentrations of oxygenated ($\Delta[HbO_2]$) and deoxygenated haemoglobin ($\Delta[HHb]$), which can be used to derive a measure of cerebral oxygenation and haemodynamic changes, with a high temporal resolution. NIRS has been used in neonatal studies as it is easy to apply on small infants undergoing intensive care. It is relatively cheap and simple when compared with other cerebral monitoring techniques, such as magnetic resonance imaging (MRI) [2]. Current research is focused on finding a robust bedside biomarker that can be indicative of brain tissue oxygenation and oxygen utilization to aid the diagnosis of brain injury and importantly to guide treatment strategies [3].

Beyond the measures of changes in HbO_2 and HHb concentrations with differential spectroscopy, more complex NIRS techniques to monitor changes in oxygenation and oxygen utilization have been implemented. Spatially resolved spectroscopy (SRS) uses multiple source-detector distances to give measurements of haemoglobin saturation often referred to as tissue oxygenation index (TOI), or regional cerebral oxygen saturation ($rScO_2$). The technique has had success as a cerebral monitor during cardiac surgery [4], however it has yet to be widely used clinically as a neuromonitoring tool in brain injury. Furthermore, the cerebral fractional tissue oxygenation extraction (cFTOE), derived from the combination of $rScO_2$ and systemic oxygen saturation (SpO_2), is also being used as a measure of oxygen consumption [5,6]. These measurements are used as a surrogate for oxygenation and oxygen utilization by many researchers; however, they are complicated parameters that can be difficult to interpret as they are affected by several different variables, and have had limited success as a biomarker for brain injury [3]. Some groups combine measurements of cerebral blood flow (CBF) and oxygenation using two optical methods, frequency-domain NIRS combined with

#214019 - $15.00 USD Received 12 Jun 2014; revised 15 Aug 2014; accepted 22 Aug 2014; published 5 Sep 2014

diffuse correlation spectroscopy (DCS), to measure the cerebral metabolic rate of oxygen ($CMRO_2$) [7,8]. While others use broadband NIRS and the optical tracer Indocyanine green (ICG) to quantify absolute CBF using the Fick principle of diffusion [9]. The combination of measures of tissue oxygenation and metabolism could potentially allow us to assess brain tissue health after injury. Towards that goal we are interested in measuring the brain tissue change in the oxidation state of the metabolic enzyme cytochrome-c-oxidase (oxCCO) and haemoglobin oxygenation with broadband NIRS.

Cytochrome-c-oxidase (CCO) is the terminal electron acceptor in the electron transport chain in mitochondria. It is responsible for more than 95% of oxygen metabolism in the body as it is essential for the efficient generation of ATP [10]. The enzyme contains four redox centers, one of which – copper A (CuA) – has a broad absorption peak in the near-infrared (NIR) spectrum which changes depending on its redox state. As the total concentration of CCO is assumed constant, the changes in the NIRS-measured oxCCO concentration are indicative of the CCO redox state and therefore provide a representation of oxygen utilization in the tissue.

Detection of CCO using NIRS is more difficult than other chromophores as its in-vivo concentration is less than 10% of that of haemoglobin and has a broad spectral signature. It has been previously demonstrated that broadband (multiwavelength) NIRS and the UCLn algorithm can accurately resolve spectral changes due to oxCCO without cross-talk from the haemoglobin chromophores [11]. There have been a few commercial systems, the NIRO 300 and NIRO 500 (Hamamatsu, Japan), that use four-wavelengths to measure the oxCCO, and we, and others, have used these previously [12,13]. However, as Matcher and colleagues reported [11], calculating Δ[oxCCO] from a small number of wavelengths can give spurious measurements and therefore it is advisable to use a broadband spectroscopy system. Our group, in a large number of studies in adult healthy volunteers during brief hypoxias and hypercapneoas, have demonstrated that is possible to measure Δ[oxCCO] with broadband NIRS independently to the hemoglobin concentration changes [14,15]. More recently, we developed a hybrid NIRS system, a combination of a lens-based broadband spectrometer and a frequency-domain spectrometer, which is capable of absolute measurements of optical absorption and scattering to measure Δ[oxCCO] and have demonstrated that scattering changes do not affect its quantification [16,17]. Another group has built a similar hybrid system to measure changes in the oxCCO signal and have demonstrated its use in preclinical studies [18]. Our interest here is to develop a portable, flexible system that can accurately measure Δ[oxCCO] in the clinical environment.

Recently in a neonatal animal model of hypoxic-ischaemia (HI), we have shown that the recovery of the broadband NIRS measurements of Δ[oxCCO] following HI correlate with the recovery in phosphorus magnetic resonance spectroscopy (^{31}P MRS) biomarkers of cerebral energy failure; this was not the case for changes in haemoglobin [19]. Bainbridge and colleagues [19] have demonstrated that, with broadband NIRS, the Δ[oxCCO] is related to cerebral tissue metabolism. Our adult brain injury studies have further shown that the CCO oxidation state is linked to the brain extracellular metabolite concentration changes measured by microdialysis during periods of hypercapnoea [15]. Therefore the NIRS Δ[oxCCO] could be a useful biomarker of metabolism in cases where other metabolic assessment methods are too invasive (e.g. microdialysis) or are difficult to perform during intensive care and have a high cost (e.g. magnetic resonance (MR) scanning) [20].

Neonatal encephalopathy (NE) affects 1-2 babies per 1000 [21] and is associated with severe neurodevelopmental problems and mortality. Most cases of NE are due to perinatal HI. Hypoxic ischaemic brain injury is an evolving process; after the initial period of energy failure during perinatal asphyxia, the cerebral metabolism typically recovers to normal for the first few hours of life but then may deteriorate, leading to a secondary energy failure which is related to the extent of brain injury or mortality [22]. Different treatment strategies to prevent the cascade of events that lead to a secondary energy failure have been trialed, but to date only therapeutic hypothermia (TH) is in routine clinical use [8,10]. The neonate is cooled to 33.5°C using a cooling mattress beginning as soon as possible in the first 6 hours of life, for

#214019 - $15.00 USD Received 12 Jun 2014; revised 15 Aug 2014; accepted 22 Aug 2014; published 5 Sep 2014

72 hours. There is an urgent need for real-time, in-vivo measurements of brain tissue oxygenation and metabolism for effective clinical assessment of these neonates during this period, especially to detect those most at risk of further brain injury and who may benefit from a redirection of clinical care, or further neuroprotective strategies.

Current methods for assessing the severity of hypoxic ischaemic brain injury include MRI, MRS, and electroencephalography (EEG). Serial EEG is a good indicator of outcome in the first 24 hours of life; very inactive or depressed EEG beyond 8-12 hours of indicates poor outcome [23]. MRI is most prognostic at around 1 week of age, but MRS provides earlier and more sensitive and specific information. Proton (^{1}H) MRS measures lactate/N acetyl aspartate (Lac/NAA), and this is the most sensitive biomarker to predict outcome. Lac/NAA correlates with the decline in cerebral energetics metabolism which lead to secondary energy failure [19]. The NIRS measured Δ[oxCCO] can also provide insight into the energetics metabolism and is suitable for cotside monitoring during TH before the MR scan at a low cost; it has the potential to provide an early insight in the 'therapeutic window' between the initial and secondary energy failure.

Here we present a new broadband NIRS system that has the ability to resolve Δ[HbO_2], Δ[HHb] and Δ[oxCCO] in neonates with NE at the cotside. We describe its use in a feasibility study and assess its potential to monitor neonatal cerebral injury. In particular we investigate and present the relationship of our broadband NIRS measurements of haemoglobin oxygenation and Δ[oxCCO] with injury severity as quantified by ^{1}H MRS Lac/NAA biomarker.

2. Methods

2.1 Study population

Ethical approval for the Baby Brain Study at University College London Hospitals Trust (UCLH), London was obtained from the North West Research Ethics Centre (REC reference: 13/LO/0106). Term infants born at or transferred to UCLH for treatment of acute brain injury were eligible for investigation; only babies without congenital malformations and considered likely to survive were considered. We present a small cohort of 6 neonates with mild to severe NE. Each subject was monitored continuously with EEG and treated with TH which was initiated within 6 hours of birth. Body temperature was lowered to 33.5°C for 72 hours, followed by a 16 hour rewarming period in which their temperature was raised by 0.5°C every 2 hours. Some (n = 4) were included in the TOBY Xe Study which is a randomized control trial of the neuroprotective effects of inhaled xenon (Xe) with hypothermia. These subjects received 30% xenon for 24 hours during the first 72 hours of life (REC reference: 10/H0707/33). Standard care in the Neonatal Intensive Care Unit (NICU) was given for all other symptoms.

Each neonate was scored using the Sarnat system which grades the severity of NE as mild (Stage I), moderate (Stage II) or severe (Stage III) based on clinical and EEG findings. In our cohort, 2 neonates were graded mild, 2 were graded moderate and 2 were graded severe. One of the severely injured neonates (002) died a few months after birth. Details of these infants are provided in Table 1.

Table 1. Clinical details of subjects studied, including days on which NIRS and MR scans were performed.

Subject	Gestational Age (weeks+ days)	Gender	Birth Weight (g)	Sarnat Grade	Treatment	NIRS (days of life)	MR scan (day of life)
002	38 + 0	Female	1770	Severe	TH + Xe	2, 3, 4, 5	5
003	41 + 0	Female	3800	Moderate	TH + Xe	1, 2, 3, 4	5
007	39 + 5	Male	3640	Severe	TH + Xe	3, 4, 5	5
008	41 + 6	Female	3498	Mild	TH + Xe	2, 3, 4, 5, 6	6
009	38 + 6	Male	2850	Moderate	TH	1, 2, 3, 4, 7	7
010	40 + 2	Female	3020	Mild	TH	2, 3, 4, 5	5

#214019 - $15.00 USD Received 12 Jun 2014; revised 15 Aug 2014; accepted 22 Aug 2014; published 5 Sep 2014

2.2 Instrumentation

A novel multi-distance broadband NIRS system, the "CYtochrome Research Instrument and appLication" (CYRIL), has been developed to measure changes in oxygenation, haemodynamics ($\Delta[HbO_2]$ and $\Delta[HHb]$) and metabolism ($\Delta[oxCCO]$) in the infant brain (see Fig. 1(a) and 1(e)). CYRIL has two channels; each channel has a single source with four detectors (see Fig. 1(b), 1(e) and 1(f)). The new system is similar to previous broadband NIRS systems that we have developed previously [14,16].

The light source is an optical fibre illuminator (ORIEL 77501, Newport, UK) with a thermally stable broadband white light source with high intensity in the NIR region. It has a 100W quartz tungsten halogen light bulb with an axial filament. The lamp output is collimated with an aspheric lens and focused onto the fibre input; a shutter and iris can be used to block or moderate the light entering the fibre. To minimize the heat deposition on the subject's head, a 610nm long-pass filter and 950nm short-pass filter were placed in the collimated region to limit the spectrum to the wavelengths detected. We have not observed any thermal effects or damage to the tissue in any of our studies.

Optical fibres and corresponding optode holders were designed to connect between the light source and the tissue, and the tissue and the spectrograph. The fibres were custom built by Loptek (GmbH, Germany) to fit the source and spectrometer at the system ends, and were made in plastic so they are light and small at the patient end to minimize discomfort. All fibre bundles are 3m in length to allow the CYRIL system to be placed at a distance from the cot. The bundles are made up of multiple high numerical aperture (NA) fibres (NA = 0.57) with diameter 30μm. The source fibre bundle branches into two fibre heads (bundle diameter 2.8mm) at the tissue. The detectors consist of eight individual fibre bundles that have a 1mm diameter. At the tissue end, each fibre has an individual plastic head of diameter 5mm (for the detectors) or 10mm (for the sources) that encases a 90° bend in the fibre to detect light on the tissue surface at a right-angle to the direction of the fibres (see Fig. 1(b)). The detector fibres can be arranged into any combination to either perform multidistance measurements (or apply SRS) or to acquire an image. The fibres are arranged vertically into a ferrule that inputs the light to the spectrometer which enables the spectrum from each fibre to be detected individually and simultaneously on the 2-dimentonal CCD chip (see Fig. 1(c)).

Optode holders were designed using AutoDesk Inventor (USA), a computer aided design (CAD) software package, and 3-dimensionally printed with the Objet500 Connex (Stratasys, USA) in a rubber-like black material (TangoBlack FLX973) that is combined with a more rigid material (VeroWhitePlus) to increase stiffness. The material is safe for application on human tissue. This design holds the source optode next to the four detector optodes horizontally with source-detector separations of 1.0cm, 1.5cm, 2.0cm and 2.5cm for multidistance measurements (see Fig. 1(b) and 1(d)).

The longest optode source-detector distance of 2.5cm was chosen to ensure a depth penetration of approximately 1cm which includes the cerebral cortex in neonates [24]. The design is small, light and flexible to consider the comfort of the subject and account for the curvature of the head. As there are two sets of optodes, the two optode holders are mirror-images of each other so that the fibres lead in the same direction from the head. For premature babies with smaller head circumferences, another optode holder was designed that uses a single source but with four detectors either side. This will allow the measurement of two hemispheres but with a smaller footprint on the head. The optodes and holder are applied to the head with a double-sided tape that is safe for human use. The tape is placed on the underside of the optode holder and then attached on the neonate's head. This procedure holds the optical fibres to the skin securely, which reduces the number of movement artefacts and optical drift from a changing position. It does not involve applying pressure to the skull to maintain optode contact to the tissue, which can result in pressure sores, so would not be suitable for long measurements.

#214019 - $15.00 USD Received 12 Jun 2014; revised 15 Aug 2014; accepted 22 Aug 2014; published 5 Sep 2014

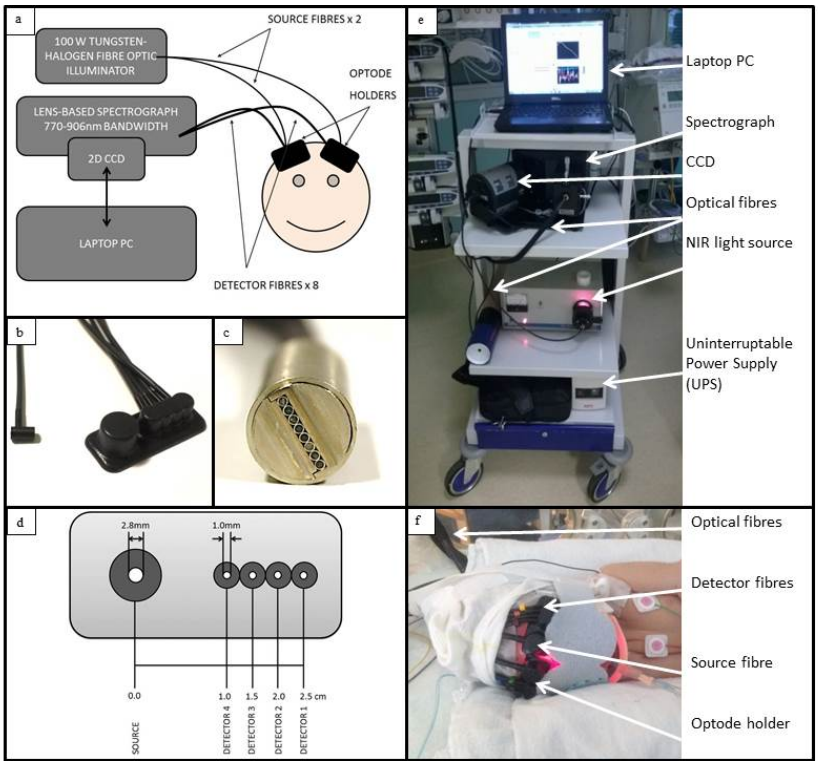

Fig. 1. a) Instrumentation diagram with experimental set up. b) Detector optode with optode holder. c) Ferrule of detector fibres for input into spectrograph vertically. d) Optode holder design with dimensions of fibre diameters (all detector fibres have the same diameter) and source-detector distances. e) Image of CYRIL system in NICU. f) Image of CYRIL optodes on a subject.

The Acton LS 785 (Princeton Instruments, USA) is a lens-based spectrograph (see schematic in Fig. 2); lens-based systems have a higher effectiveness than mirror-based spectrographs with respect to the throughput of light (over 99% transmission throughout the entire working range of the spectrograph). The light collected from the tissue surface by the detectors inputs into fibre-adapted entrance and passes through a variable slit which prevents overexposure. We found the optimal slit opening to be 20μm. The light is collimated to reduce loss and then is incident upon a diffraction grating. This grating is blazed at 1000nm and has 830 grooves per mm which gives a wavelength resolution of 0.7nm and 136nm bandwidth. As the grating is mounted on a rotating platform, it is possible to select the range of wavelengths that we resolve; the 770nm-906nm range was chosen as oxCCO is a strong absorber at 830nm [25]. Previous in-house systems built to measure oxCCO have used the 780-900nm range successfully [26]. After diffraction at the grating, the light is focused onto the CCD detector with an f/2 focusing lens. Focusing the light in the y-direction reduces cross-talk between the detector channels.

#214019 - $15.00 USD Received 12 Jun 2014; revised 15 Aug 2014; accepted 22 Aug 2014; published 5 Sep 2014

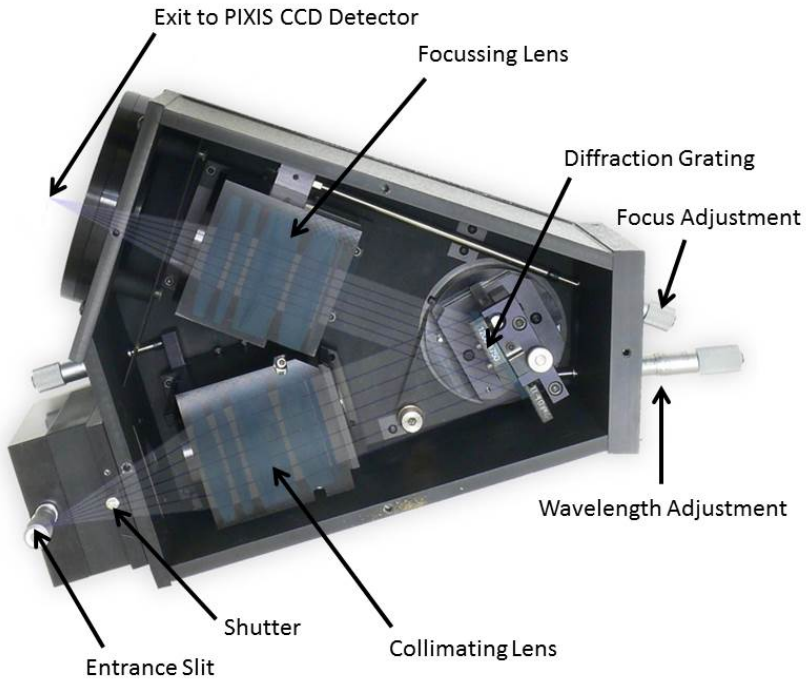

Fig. 2. Acton LS 785 Spectrograph (Princeton Instruments, USA).

The PIXIS 512f CCD camera (Princeton Instruments, USA) has a 2-dimension array of 512 x 512 detector pixels on a 12.3mm x 12.3mm chip and each pixel is 24μm x 24μm. The 2-dimensional chip allows light from all 8 detector fibres to be detected simultaneously. It is a front-illuminated CCD which is optimal for the moderate to low light levels of NIRS, and the peak quantum efficiency is within the NIR region. The CCD is cooled to −70°C (thermally stable to ± 0.05°C) during operation to reduce dark count, at this temperature the dark current is 0.002 electrons per pixel per second. The CCD read noise at 1000kHz is 5 electrons root mean square (RMS). The CCD has a USB 2.0 data interface for control and acquisition with a laptop. Each pixel in the x-direction was calibrated to its corresponding wavelength bin using LightField (Princeton Instruments, USA) acquisition software with the IntelliCal calibration package. The CCD resolution after calibration is 0.27nm. Therefore our system has a wavelength resolution of 0.27 ± 0.70nm. Table 2 has a summary of the specifications of the spectrometer (spectrograph combined with the CCD).

A program was created in LabVIEW 2011 (National Instruments, USA) to control the CCD, collect the raw data and calculate the corresponding concentrations using the modified Beer-Lambert Law (as defined in 2.3 Algorithm). The program has a graphical user interface (GUI) that allows the user to view the detected intensity spectra and concentration changes of the chromophores per channel in real-time at the bedside. The program has a wavelength binning functionality that allows the user to take and display an intensity weighted image of the CCD pixel array and then choose the region of interest (ROI) for each horizontal strip to bin (see Fig. 3). Each strip is related to one of the detector fibres that are input into the spectrometer. The strips can be adjusted to maximize the intensity spectra per channel without saturation and limit cross-talk between channels; significant cross-talk is not observed in our set-up. The CCD is programmed to acquire data per the settings described by the user using LabVIEW drivers for the PIXIS 512f CCD (Scientific Imaging Tool Kit, R Cubed Software, USA). The CCD collects data separately from the ROIs and bins the data by wavelength. The

#214019 - $15.00 USD Received 12 Jun 2014; revised 15 Aug 2014; accepted 22 Aug 2014; published 5 Sep 2014

intensity spectra for each ROI are displayed in the GUI and the user can move between the tabs to view each detector channel. The magnitude of light intensities recorded peaked at >60000 counts per second, typical photon counts were >50000 for the detectors 1cm from the source, >35000 for the 1.5cm detectors, >30000 for the 2.0cm detectors, and >24000 for the 2.5cm detectors. The dark count was 2 orders of magnitude lower at ~400 counts.

The raw data (intensity spectra), processed data (differential concentrations) and time log are saved as comma-separated value (csv) files in real-time immediately after the data has been processed for each measurement. The new measurement is appended to the csv file to ensure that the data is saved in real-time which will prevent loss of data in the event of a computer failure. The chromophore concentration changes are displayed in the GUI in real-time and the user can choose which channel to display and how many of the recent data points are displayed. However in order to minimize the amount of data kept in random access memory (RAM) and therefore reduce the processing time, it is advisable to limit the number of measurements displayed.

CYRIL is able to successfully record data continuously at 1Hz for long periods (>24 hours) without error. CYRIL is a compact and portable system that can be moved to the cotside without hindering access to other equipment or the cot itself. Artefacts from light, movement and poor optode-tissue contact are common in a clinical environment and must be removed before the data is used. We have characterized such artefacts by deliberately inducing them to aid awareness and prevention, and also to improve removal.

After the measurements, reference spectra should be acquired with CYRIL to characterize the intensity spectrum of the light through the system without attenuation through tissue. A poster tube lined with optically black rubberized fabric is used to collect the spectra, each source and detector pair are placed either end of the tube. Each reference spectrum is collected and averaged over a period of ~10s.

Table 2. Summary of spectrometer (combined spectrograph and CCD) specifications.

Specification	
Light throughput	99.4%
Bandwidth	136nm
Spectral range	770-906nm
Spectral resolution	0.27 ± 0.70nm
CCD chip size	12.3mm x 12.3mm
CCD pixels	512 x 512
CCD temperature	−70°C ± 0.05°C
Dark current	0.002 e^-/p/s
Read noise	5 e^- RMS

2.3 Algorithm

The changes in chromophore concentrations were calculated from the measured changes in broadband NIR light attenuation using the modified Beer-Lambert law as applied with the UCLn algorithm first described by Matcher et al. [11]. The UCLn algorithm is a least-squares fitting procedure that based on multiple regression analysis, using the Beer-Lambert law to determine the best fit of the chromophore extinction coefficients, ε, to the measured attenuation changes, ΔA, over n number of wavelengths, λ:

$$\begin{bmatrix} \Delta[HbO_2] \\ \Delta[HHb] \\ \Delta[\text{oxCCO}] \end{bmatrix} = \frac{1}{pathlength} \begin{bmatrix} \varepsilon_{HbO_2}(\lambda_1) & \varepsilon_{HHb}(\lambda_1) & \varepsilon_{oxCCO}(\lambda_1) \\ \varepsilon_{HbO_2}(\lambda_2) & \varepsilon_{HHb}(\lambda_2) & \varepsilon_{oxCCO}(\lambda_2) \\ \vdots & \vdots & \vdots \\ \varepsilon_{HbO_2}(\lambda_n) & \varepsilon_{HHb}(\lambda_n) & \varepsilon_{oxCCO}(\lambda_n) \end{bmatrix}^{-1} \begin{bmatrix} \Delta A(\lambda_1) \\ \Delta A(\lambda_2) \\ \vdots \\ \Delta A(\lambda_n) \end{bmatrix}. \quad (1)$$

#214019 - $15.00 USD Received 12 Jun 2014; revised 15 Aug 2014; accepted 22 Aug 2014; published 5 Sep 2014

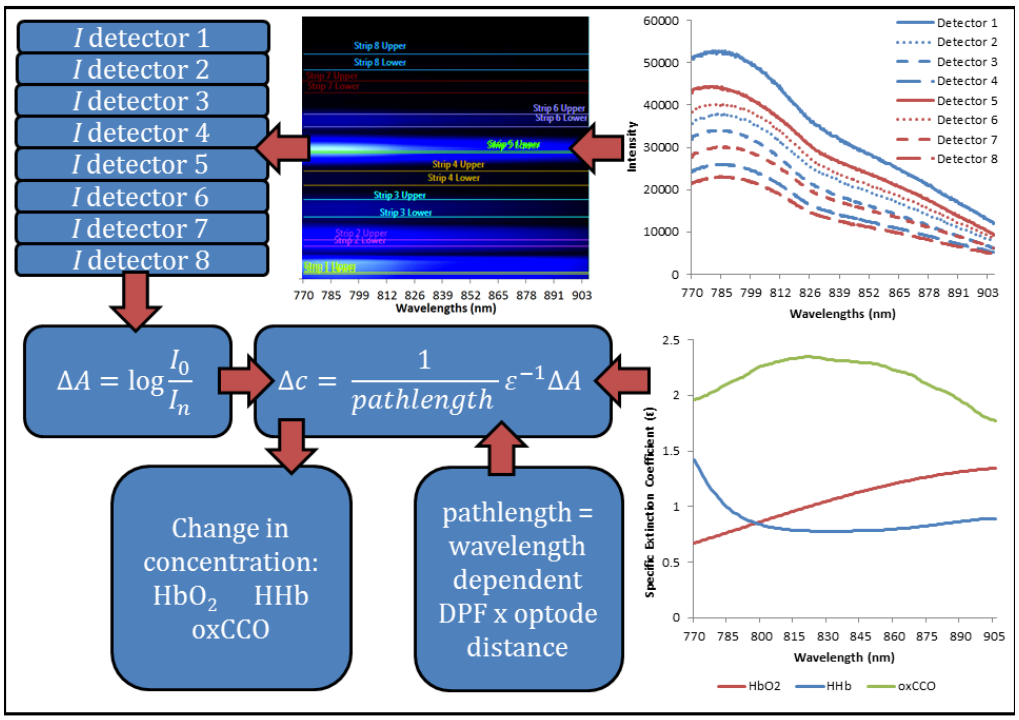

Fig. 3. Schematic showing modified Beer-Lambert law and the input variables. Intensity spectra, I, are recorded simultaneously at all detectors (red = left side channel (detectors 1 to 4), blue = right side channel (detectors 5 to 8)) and the ROIs of each detector are binned. The intensity spectra are converted to change in attenuation, ΔA, and the change in concentration changes, Δc, are calculated using the UCLn algorithm with the specific extinction coefficient of the chromophores, ε, and the pathlength.

The differential attenuation is calculated and interpolated to the nearest nanometer across 770-906nm using a spline interpolation. The UCLn algorithm was used to solve for $\Delta[HbO_2]$, Δ[HHb] and Δ[oxCCO] across these 136 wavelengths. The specific extinction coefficient spectra used are provided in Kolyva et al. [26]. The optical pathlength was derived from the product of the distance between the optodes and the differential pathlength factor (DPF), which was has been previously measured as 4.99 (± 9%) on the head of a newborn infant [27], corrected for the wavelength-dependency of the DPF. The measured concentration changes presented are taken from the longest source-detector distance (2.5cm) as measurements from the furthest detector are more likely to reflect cerebral changes. Figure 3 shows a schematic of the algorithm with the input variables.

2.4 Protocol

The CYRIL NIRS measurements were collected continuously over periods from 1 to 15 hours during the first 6 days of life at a sampling frequency of 1Hz. All measurements were taken bilaterally on the forehead over the frontal lobe (see Fig. 1). NIRS measurements began as soon as consent was granted from the parents, with a view to acquiring data as close to birth as possible. Data were recorded on each day of life from the start of consent until the MR scan, this occurred between 5 and 7 days of life. Final NIRS measurements were performed immediately before or after the MR scan. Table 1 shows the timings of the NIRS and MR recordings per subject.

Systemic data from the Intellivue Monitors (Philips Healthcare, UK) were collected using an application called ixTrend (ixellence GmbH, Germany). Signals recorded include oxygen

#214019 - $15.00 USD Received 12 Jun 2014; revised 15 Aug 2014; accepted 22 Aug 2014; published 5 Sep 2014

saturation (SpO_2) measured by pulse oximetry on the foot or hand, heart rate (HR) by electrocardiograph (ECG), mean arterial blood pressure (MABP) from an intra-arterial catheter, and transcutaneous carbon dioxide (CO_2) tension.

Continuous and amplitude integrated EEG (aEEG) were recorded from arrival to the NICU until the infant was rewarmed following TH. The babies spent one hour in the MR scanner usually after rewarming. MR scans included a measurement of Lac/NAA with hydrogen (^1H) MRS.

2.5 Data analysis

Data analysis was carried out in MATLAB (Mathworks, USA). NIRS data were processed with an automatic wavelet de-noising function which reduces the high frequency noise but maintains the trend information. Systemic data were down-sampled and interpolated to the NIRS data timeframe (1Hz). Artefacts from movement or changes in external lighting were removed using the method suggested by Scholkmann et al. [28] which is based on moving standard deviation and spline interpolation. This method also corrects shifts in the baseline due to artefact.

To investigate the spectral changes due to the oxCCO chromophore, the UCLn algorithm was also used to derive changes in chromophore concentrations when solving only for the other 2 chromophores (HbO_2 and HHb). Attenuation-change spectra were then back-calculated from these concentration changes and the differences between the 2- and 3-chromophore fits were studied. If we are fitting all of the chromophores that explain our spectra then the residual error between the two sets should not have a defined shape, however if there is a shape to the spectra then this would suggest that there is a chromophore that is unaccounted for.

In our previous studies of animal models of NE [19], Δ[oxCCO] is measured prior to, during and after the asphyxia, so that changes in concentration during these conditions have biological significance . In human subjects, measurements can only be performed post-insult. Therefore we do not have a pre-insult baseline from which to measure changes and we have less information on how the cerebral metabolism has responded to the primary insult. Therefore we are interested in large global physiological events, such as spontaneous oxygen desaturations, to observe how the cerebral metabolism responds to, or recovers from, a systemic change, and whether this response differs between a poor and a good outcome.

There were a total of 21 data sets from the cohort of 6 subjects. The length of the data sets ranged from 11 minutes to 15 hours. All data sets included continuous measurement of $\Delta[HbO_2]$, Δ[HHb], Δ[oxCCO], SpO_2, HR, and CO_2 tension. We used Δ[HbD] (= $\Delta[HbO_2]$ - Δ[HHb]) as a surrogate market of oxygen delivery as it represents the mismatch between $\Delta[HbO_2]$ and Δ[HHb], and Δ[HbT] (= $\Delta[HbO_2]$ + Δ[HHb]) as an indicator of brain blood volume changes. Only 3 of the 6 subjects had MABP recorded continuously. Data was analysed according to decreases in the SpO_2 signal and the changes in the other variables were recorded over this event. The magnitude of changes in all variables was recorded for every SpO_2 desaturation of greater than 5%, as smaller changes may not be clinically significant. The SpO_2 desaturation start and nadir were identified and selected manually; these time points were then use to calculate the changes in $\Delta[HbO_2]$, Δ[HHb] and Δ[oxCCO] over this period. See Fig. 4 for a schematic of this process. Magnitude changes in $\Delta[HbO_2]$, Δ[HHb] and Δ[oxCCO] were recorded for both NIRS channels on the left and right side of the forehead, which were placed above the frontal lobes of right and left hemispheres respectively, and then these changes were averaged. The change of MABP, HR and CO_2 tension in the period between SpO_2 desaturation start and nadir were also recorded with the standard deviation.

2.6 Statistical analysis

All statistical analysis was carried out in MATLAB (Mathworks, USA). The Pearson correlation coefficients, r, were calculated between the magnitudes of each of SpO_2 saturation changes and the corresponding changes in Δ[HbD], Δ[HbT] and Δ[oxCCO] for each subject

#214019 - $15.00 USD Received 12 Jun 2014; revised 15 Aug 2014; accepted 22 Aug 2014; published 5 Sep 2014

across all days. This was also performed for Δ[oxCCO] against Δ[HbD] and Δ[HbT].These coefficients were then correlated with the Lac/NAA measurement for each subject to identify trends between the NIRS measured values and the severity of injury. P-values of less than 0.05 were considered statistically significant.

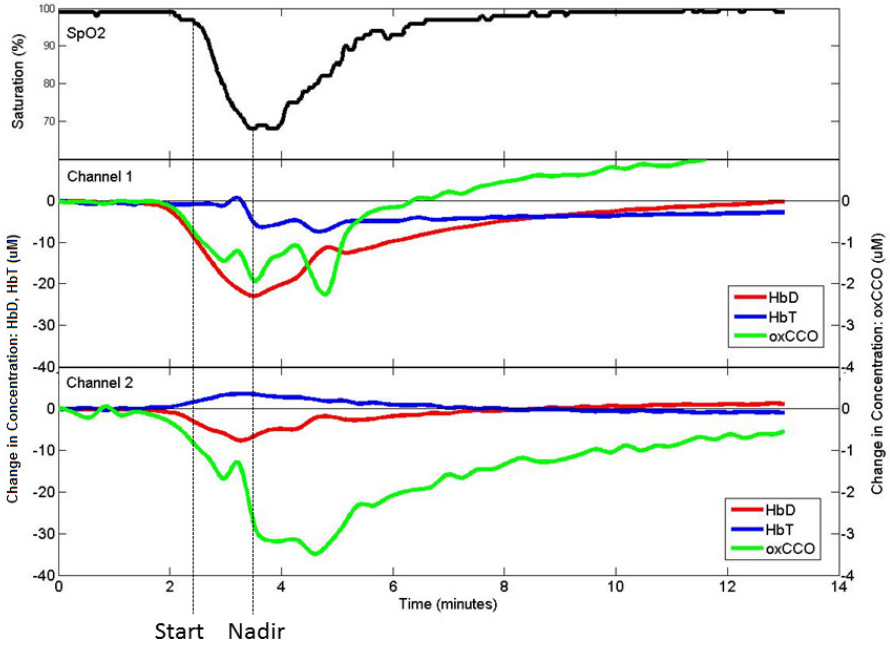

Fig. 4. Example of SpO_2 desaturation from channel 1 (left side) and channel 2 (right side) on subject 003 with start and nadir of desaturation marked for SpO_2 and corresponding position in NIRS signals.

3. Results

3.1 Measurement of Δ[oxCCO]

NIRS signals were recorded in 6 subjects for a total of 212 hours and 25 minutes. Figure 5 shows examples of the intensity spectra recorded (Fig. 5(a)) and the corresponding change in attenuation between them (Fig. 5(b)). The change in the shape of the intensity spectrum reflects the change in the levels of chromophore concentration in the tissue; during SpO_2 desaturation the peak of the spectra shifts from ~780nm to ~785nm due to the decrease in $\Delta[HbO_2]$ and Δ[oxCCO], and the increase in Δ[HHb]. An example of change in chromophore concentrations during a desaturation event can be seen in Fig. 4.

#214019 - $15.00 USD Received 12 Jun 2014; revised 15 Aug 2014; accepted 22 Aug 2014; published 5 Sep 2014

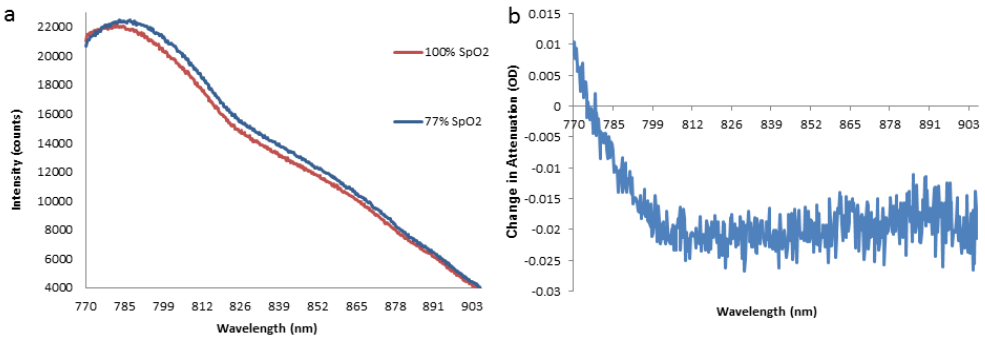

Fig. 5. a) Example of intensity spectra before desaturation (SpO_2 = 100%) and at the nadir of desaturation (SpO_2 = 77%) in subject 003, left side channel, from the longest source-detector distance. A shift in the peak of the spectrum is observed. b) Change in attenuation between intensities shown in a) – this relates to $\Delta[HbO_2]$ = ~-6 μM, Δ[HHb] = ~3 μM and Δ[oxCCO] = ~-1.5μM.

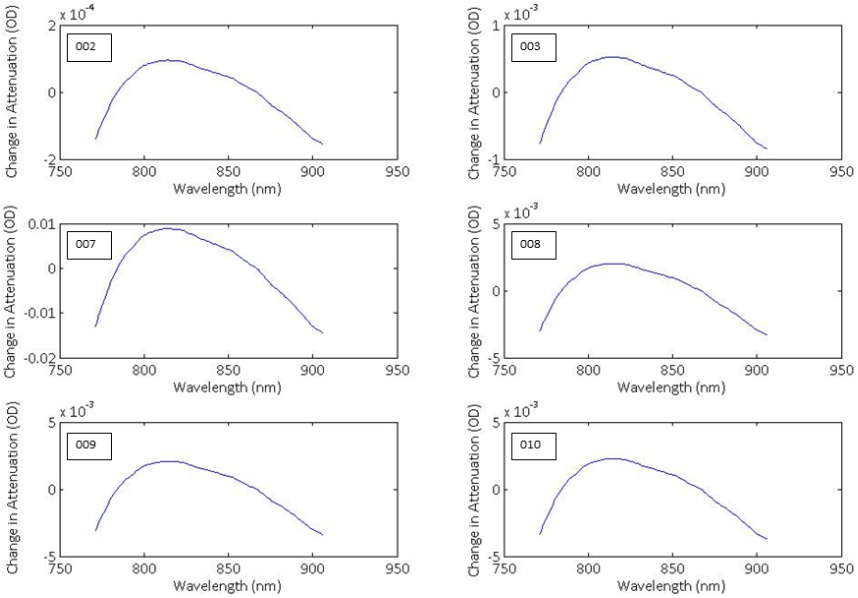

Fig. 6. Attenuation-change spectra back-calculated from the calculated concentration changes during the largest SpO_2 desaturation observed in each subject (subject number labelled on graphs). The presented spectra are the average of all spectra during the desaturation on the left side channel. The difference between the 3- and the 2-chromophore fit is plotted.

The back-calculated attenuation-change spectra from the furthest detector are shown in Fig. 6 as the difference between the 3- and the 2-chromophore fit for the each of the 6 subjects during their largest desaturation. It is noted that the spectrum presented for each subject is an average spectrum, derived from all individual spectra corresponding to the largest desaturation event in that subject. The spectra do not have an arbitrary distribution around y = 0, but appear to show a shape approximating the oxidised minus reduced CCO spectrum (see Fig. 3), featuring a broad peak at approximately 830 nm. This suggests that fitting the measured changes in near-infrared attenuation only for HHb and HbO_2 would leave a chromophore with the spectral features of oxCCO unaccounted for. Based on these findings, only results from the 3-chromophre fit are discussed throughout this study.

#214019 - $15.00 USD Received 12 Jun 2014; revised 15 Aug 2014; accepted 22 Aug 2014; published 5 Sep 2014

3.2 Multimodal data analysis

A total of 236 SpO_2 desaturations from 6 subjects and 212 hours and 25 minutes of data were identified. Desaturations occurred over periods from 2 seconds up to 28 minutes and the mean desaturation was −12 ± 3%. Table 3 shows the mean SpO_2 changes during the desaturation per subject and across all subjects, with corresponding mean variations (± standard deviation) in systemic (MABP, CO_2, HR) and NIRS signals. On average the MABP and CO_2 tension signals decreased by 0.9 ± 1.6mmHg and 0.4 ± 1.1kPa respectively. The HR signal increased by 1.4 ± 2.6bpm. There was a consistent negative change in the Δ[HbD] and Δ[oxCCO] measurements, mean decreases were 3.0 ± 1.7μM and 0.22 ± 0.11μM, and a positive change in the Δ[HbT] measurements across all subjects, mean increase was 0.85 ± 0.58μM.

Pearson correlation coefficients, r, between the magnitudes of each of SpO_2 saturation changes and the corresponding changes in Δ[HbD], Δ[HbT] and Δ[oxCCO], and for Δ[oxCCO] against Δ[HbD] and Δ[HbT] are presented in Table 4. These coefficients were then correlated with the corresponding Lac/NAA measurement across all subjects, which are displayed in the final row of Table 4. The correlation coefficients between Δ[HbD] and Δ[oxCCO] have a statistically significant ($p<0.01$) correlation with the MRS-measured Lac/NAA values (Table 5).

Table 3. Number of desaturations, n, and mean ± standard deviation (SD) (to 2 significant figures) for all systemic variables during the desaturations per subject, and across all subjects. Thalamic Lac/NAA measured by MRS. Changes in MABP were not available (N/A) for 3 of the 6 subjects.

Subject	n	ΔSpO_2 (%)	ΔMABP (mmHg)	ΔCO_2 (kPa)	ΔHR (bpm)	Δ[HbD] (μM)	Δ[HbT] (μM)	Δ[oxCCO] (μM)	Lac/NAA
002	33	−13±11	1.2±0.9	−0.61±0.57	0.16±0.71	−2.4±6.6	0.45±3.4	−0.02±0.63	0.20
003	70	−17±19	−2.6±6.0	0.41±0.17	0.35±2.5	−6.5±10.5	1.4±3.5	−0.37±1.1	0.16
007	7	−9.6 ± 3.8	N/A	−2.8±1.8	−0.5 ±2.6	−1.3±3.3	0.30±1.2	−0.22±0.33	1.32
008	30	−9.4±9.6	N/A	0.23±0.09	5.2±5.1	−2.0±3.4	0.94±3.7	−0.18±1.1	0.17
009	25	−11±5	−1.3±2.2	0.03±0.24	4.8±5.3	−2.3±6.2	1.8±1.9	−0.29±0.50	0.16
010	71	−10±5	N/A	0.12±0.08	−1.5±3.7	−3.5±4.4	0.2±3.3	−0.28±1.1	0.15
All	236	−12±3	−0.9±1.6	−0.4±1.1	1.4±2.6	−3.0±1.7	0.85±0.58	−0.22±0.11	

Table 4. Pearson correlation coefficients (r) of magnitude of changes in >5% SpO_2 desaturations for each subject across all days. *p<0.05, **p<0.01.

Subject	SpO_2 vs. HbD	SpO_2 vs. HbT	SpO_2 vs. oxCCO	HbD vs. oxCCO	HbT vs. oxCCO
002	0.92**	−0.38*	−0.38*	0.05	0.40*
003	0.93**	−0.47**	0.52**	0.55**	0.25*
007	0.59	−0.49	0.45	0.89*	−0.67
008	0.05	0.20	0.15	0.47**	0.69**
009	0.62**	−0.43*	−0.35	−0.10	0.58**
010	−0.13	−0.11	−0.18	0.16	0.74**

Table 5. Pearson correlation coefficients, r, from magnitude of changes during oxygen desaturations correlated against MRS-measured Lac/NAA ratio. **p<0.01.

Thalamic Lac/NAA vs.	*r*
SpO_2 vs. HbD	−0.06
SpO_2 vs. HbT	0.52
SpO_2 vs. oxCCO	0.42
HbD vs. oxCCO	0.91**
HbT vs. oxCCO	0.28

#214019 - $15.00 USD Received 12 Jun 2014; revised 15 Aug 2014; accepted 22 Aug 2014; published 5 Sep 2014

4. Discussion

We have developed a new clinical instrument based on a lens-based broadband spectrometer capable of recording multispectral NIR intensity data at multiple channels. We have demonstrated the use of CYRIL in the NICU for continuous periods over 1-5 days, recording from 1 hour up to 16 hours per day, to simultaneously measure changes in cerebral oxygenation, haemodynamics and [oxCCO] in 6 newborn infants. We have also performed a feasibility study to assess the clinical significance of the haemodynamic and metabolic information from CYRIL and have found significant association with known biomarkers of NE as measured by ^{1}H MRS. To our knowledge this is the first time that the in-vivo oxidation changes of brain tissue CCO have been recorded in NE infants in the NICU.

Previous measurements of Δ[oxCCO] have been criticized as cross-talk from the haemoglobin chromophores. The effect of haemoglobin cross-talk was not evident in our data. Spectroscopic cross-talk is demonstrated as a change in one chromophore mimicking the change in another [29], but it has been shown that the broadband NIRS-measured Δ[oxCCO] signal cannot simply be explained by this cross-talk effect [30]. We have validated the independence of the Δ[oxCCO] signal by finding the difference between the back-calculated attenuation spectra from the 2- and 3-chromophore fit algorithms (Fig. 6). This suggests that fitting the measured changes in near-infrared attenuation only for HHb and HbO_2 would leave a chromophore with the spectral features of oxCCO unaccounted for. This method has been used by us [31] and others [32] to validate measurements of oxCCO previously.

NIRS systems have intrinsic problems with movement and ambient light artefacts due to their high sensitivity [28]. Movement of the head or optodes cause changes in the light coupling to the tissue and large changes in ambient light intensity can saturate the CCD detector as the system is sensitive to low light intensities. Our system is not immune to these problems; however, we have characterized these events in the clinical environment by inducing movement or light changes to gain knowledge about how their occurrence can be prevented, and how they artefacts can be identified in, and then removed from, the data. Through this work, we identified the most disruptive white light source that was used in clinical care. This light source was replaced with a light with a spectrum that peaks around 500nm (blue end of white light spectrum) so does not affect our measurement as the system has a bandwidth of 770-906nm.

The spectrograph and CCD used in CYRIL has enabled us to measure low-concentration chromophores due to the high light throughput, resolution and signal-to-noise ratio; however, there are alternative broadband spectrometers available that could be used to measure oxCCO. Off-the-shelf micro-spectrometers, such as the QE65000 (Ocean Optics, USA), can be modified to perform tissue spectroscopy by improving the light collection with custom-built fibres and entrance slit removal [33]. These low-cost and small-footprint instruments have been shown to successfully recover changes in tissue chromophore concentrations from layered phantoms [34] and in vivo [33]. Another group has used larger Czerny-Turner (mirror-based) systems to resolve for other low-concentration mitochondrial chromophores [35].

The changes observed in the NIRS signals during spontaneous SpO_2 desaturations varied between subjects, however the mean values for Δ[HbD] and Δ[oxCCO] consistently decreased during desaturation and Δ[HbT] consistently increased which is expected as cerebral blood flow and Δ[HbT] increases during hypoxia in the healthy brain [14] (see Table 3). The correlation between the magnitude of changes of SpO_2 and Δ[HbD] was positive for 5 of the 6 subjects, and statistically significant for 3 of those. The r values tended to be higher in neonates with severe or moderate NE, which suggests that the relationship between systemic and cerebral oxygenation was more coupled in these cases. The correlation between the magnitude of changes of SpO_2 and Δ[HbT] was negative for 5 of the 6 subjects. Significant correlation was found in the same 3 subjects as with Δ[HbD] and SpO_2 so the decrease in cerebral oxygenation was combined with an increase in total haemoglobin during the desaturation events in the more severely injured infants.

#214019 - $15.00 USD Received 12 Jun 2014; revised 15 Aug 2014; accepted 22 Aug 2014; published 5 Sep 2014

The correlation between the magnitude of changes of SpO_2 and Δ[oxCCO] during desaturations was varied; half of the subjects had negative correlations and half had positive, two were statistically significant correlations – one positive, one negative. This suggests that different neonates have different metabolic responses to these events, despite having similar haemodynamic responses. One might expect that the correlation between the changes in Δ[oxCCO] and cerebral oxygenation (Δ[HbD]) would be similar to that of Δ[oxCCO] and systemic oxygenation (SpO_2); however this is not the case as the strength and direction of the correlation differs per subject. This perhaps emphasizes the fact that systemic arterial oxygenation at certain instances is not a good indicator of regional brain tissue oxygenation. The correlation between the changes in Δ[HbT] and Δ[oxCCO] changes is the most consistent with 5 out of 6 subjects having a significant positive correlation, the other (007) is negative and not significant, however this could be due to the low number of desaturations observed in that subject (n = 7). The Δ[HbD] and Δ[oxCCO] r values are significantly associated with the thalamic Lac/NAA ratio ($p<0.01$) which suggests that a highly coupled cerebral oxygenation and metabolism is indicative of a more severe brain injury. Our data shows that in more severely injured neonates the magnitude of the drop in Δ[oxCCO] correlates highly with the magnitude of the Δ[HbD] drop during systemic oxygen desaturations. This suggests a tight coupling between the oxygen delivery and oxygen utilization in these infants.

Banaji et al. predicted how the Δ[oxCCO] signal should respond during an oxygen desaturation using a mathematical model of brain circulation and energy metabolism [36]. During hypoxia in a healthy, 'normal' brain there is an approximately linear relationship with HbO_2. When the metabolic rate and cerebral blood flow is lowered however, the relationship becomes bi-phasic. This work shows that the relationship between Δ[oxCCO] and Δ[HbD] could depend on the neurological health of the brain, as we suggest here. Our previous studies of hypoxaemia in awake, healthy, young adults reported correlation between Δ[oxCCO] and cerebral oxygen delivery during the oxygen desaturations, but did not find a relationship between Δ[oxCCO] and Δ[HbD] [14].

To our knowledge, Δ[oxCCO] has not been measured in human neonates with NE before, however Edwards et al. studied the chromophore during spontaneous desaturations in newborn infants with no evidence of brain injury and found no relationship between Δ[oxCCO] and SpO_2 over small (3-11%) changes in SpO_2 [37]. They concluded that cerebral haemodynamic changes more readily affect Δ[oxCCO] than systemic oxygenation which agrees with our findings. Our group has recorded NIRS-measured Δ[oxCCO] in controlled preclinical animal models of NE [19]. The recovery of the Δ[oxCCO] signal after NE was shown to correlate with the nucleotide triphosphate to exchangeable phosphate pool ratio (NTP/epp) which is a ^{31}P MRS-measured biomarker of NE and is related to Lac/NAA. This feasibility study suggests that this finding is translatable from the piglet model to the human neonate.

There have been a few recent studies of NE with NIRS. Dehaes et al. [8] found that $CMRO_2$ and CBF was significantly lower in neonates during TH compared with post-TH and age-matched controls. This finding agrees with Wintermark et al. [38] who reported that newborns with severe NE had lower CBF and seemed to extract less oxygen. The reduction in metabolic rate in the most severely asphyxiated newborns may reflect mechanisms to minimize further injury. This could either be a manifestation or the cause of the underlying severity of NE. Both of these studies noticed elevated tissue oxygen saturation in newborns with more severe NE which suggest that they were extracting less oxygen.

It should be noted that the NIRS measurements were taken from above the frontal lobe, whereas the MRS-measured Lac/NAA was from the thalamus. Thalamic Lac/NAA was used as our marker of NE severity however it does not give the complete picture of the brain injury as the pathology is not always global so a subject with injury in the white matter may not have a high Lac/NAA ratio in the thalamus. This may explain the incongruity observed in subject 002 – a Lac/NAA measurement of 0.20 when the injury was severe; this is much lower than the Lac/NAA value of 1.32 measured in the other severe NE case (007).

#214019 - $15.00 USD Received 12 Jun 2014; revised 15 Aug 2014; accepted 22 Aug 2014; published 5 Sep 2014

The spontaneous desaturations in systemic oxygen may have occurred for a variety of reasons; none were recorded during seizures. The changes in cerebral oxygenation and oxygen utilization we recorded will vary depending on the cause of the desaturation, and the other physiological changes such as CO_2, HR and MABP which were not corrected for in this study, but were generally of low values during the desaturations studied. CO_2, HR and MABP have a large effect on the cerebral oxygenation and metabolism [36], so in future work we will use a method that considers multiple systemic variables, for example, canonical correlation analysis [39] or mixed model analysis [14]. We will also investigate differences between the days of measurements and treatments (i.e. during or post-TH). We are continuing to study further subjects and will expand our analysis to these neonates.

Our system has the capacity for SRS measurements to derive haemoglobin saturation using the multiple detectors per channel [40]. We plan to apply this technique to the data already recorded to calculate absolute measurements of haemoglobin saturation, such as TOI. Multidistance measurements can also be used to separate changes in the superficial layers above the cerebral cortex using a two-layer model [41], we will also investigate the application of this method to our current and future data. In addition, we also have the capacity to perform imaging with a different arrangement of the detector fibres; the combination of the multiple individual detector optodes and 3-dimensional printing to create optode holders means that the system is flexible to imaging as well as spectroscopy.

5. Conclusion

We have developed and described a new broadband NIRS system called CYRIL to simultaneously measure the changes in cerebral tissue oxygenation, haemodynamics via estimation of the changes in haemoglobin concentrations; in addition to metabolism and oxygen utilization via the measurement of the oxidation state of CCO. We have used CYRIL in the newborn infant with neonatal encephalopathy in the NICU for continuous periods over up to 5 days.

NIRS data was collected simultaneously with systemic data to allow multimodal data analysis. This allowed us to study the NIRS variables in response to global pathophysiological events and we have focused our analysis to spontaneous oxygen desaturations. We have shown with a feasibility study in 6 NE infants that the relationship between haemoglobin oxygenation changes and cytochrome-c-oxidase oxidation changes during these desaturation events was significantly correlated with the MRS-measured Lac/NAA biomarker of injury severity.

Acknowledgments

The authors would like to thank the parents who gave consent for their children to participate in this study. This research was funded by The Wellcome Trust, grant 088429/Z/09/Z, and the UCL-Cambridge Centre for Doctoral Training in Photonic Systems Development, Engineering and Physical Sciences Research Council, grant EP/G037256/1. NR, SM and JM acknowledge the support of the UCL/UCLH Biomedical Research Centre.